ORIGINAL RESEARCH ARTICLE

Reaction Mechanisms During Melting of H-DRI Focusing on Slag Formation and the Behavior of Vanadium

AMANDA VICKERFÄLT, JOAR HUSS, JOHAN MARTINSSON, and DU SICHEN

The reaction mechanisms during melting of hydrogen direct reduced iron pellets (H-DRI) with different degrees of reduction were studied experimentally at 1773 K to 1873 K at different times (60 to 600 seconds), focusing on the autogenous slag formation. It was found that an autogenous slag is formed inside the pellets prior to the melting of the metal phase. The formation of the autogenous slag started with the melting of FeO, initially located in the center of the iron grains. The liquid FeO flowed into the pore network of the pellet. While flowing, the liquid FeO dissolved parts of the residual oxides, forming an autogenous slag. The slag stayed in the pore network until the iron was molten. Upon melting of the iron, the slag coalesced into spherical droplets. The final state is reached upon the separation of the metal and slag phases by flotation, as a bulk slag was formed on the surface of the liquid iron. In addition, since the iron ore used in this study contains vanadium, the behavior of V was discussed separately based on the experimental observations to build a basis for future studies on V extraction.

https://doi.org/10.1007/s11663-023-02827-z

I. INTRODUCTION

MANY steel producers are dependent on virgin iron based on iron ore to meet their high-grade steel requirements. Iron ore is made into steel primarily through the blast furnace–basic oxygen furnace route, which is the dominating steelmaking route. Huge amounts of CO_2 emissions are associated with this production route, mainly due to the use of coke as reductant in the blast furnace.[1] As environmental aspects have become more and more important in society, governments all over the world have set targets to reduce the industrial environmental impact, for example, the Paris agreement and UN sustainability goals. Many steel producers have therefore begun a journey toward fossil-free steelmaking, decreasing their carbon footprint.[2,3] A promising alternative to the blast furnace route has been found to be adjust the existing direct reduction shaft furnaces that use natural gas to reduce the iron ore, to instead use higher fraction, or even pure, hydrogen as reductant. Employing direct reduction shaft furnaces using H_2 as reductant produces H_2O as byproduct instead of CO_2. The sustainability of this process is dependent on the access to hydrogen produced by renewable energy sources.[4] The iron product, hydrogen direct reduced iron (H-DRI), is a solid product that can be melted in an electric arc furnace (EAF). The use of H-DRI affects the EAF process route,[5] making fundamental understanding related to melting and refining of H-DRI increasingly important. The most important reason being to optimize the cost of steelmaking to cover the high costs associated with green hydrogen electrolysis.[6] H-DRI will most likely be fed to the EAF continuously rather than in batches. The melting of H-DRI will be affected by slag composition, local temperature, and the pellets' contact to the slag and/or steel bath.

H-DRI contains iron and several types of oxides originating from gangue, flux, and incomplete reduction of iron oxide. Unlike in pig iron from the blast furnace, constituents such as Si, Mn, V, and P (when occurring in apatite) remain oxidic in H-DRI.[7,8] The unreduced oxides form a so-called autogenous slag when the H-DRI is melted.[9] Two prior studies within the present research group have studied the behavior of the unreduced oxides during melting.[10,11] It was found that the fine mix of oxides together with increased CaO additions in the pellet provide efficient P refining during batch melting of pellets.[10] The dephosphorization has been thoroughly studied earlier and is not part of this work.[11] These studies show that the autogenous slag

AMANDA VICKERFÄLT, JOAR HUSS, and JOHAN MARTINSSON are with the Swerim AB, Box 7047, 164 07 Kista, Sweden. Contact e-mail: johan.martinsson@swerim.se DU SICHEN is with the KTH Royal Institute of Technology, 100 44, Stockholm, Sweden and also with the Hybrit Development AB, Box 70359, 107 24 Stockholm, Sweden.

Manuscript submitted January 17, 2023; accepted May 15, 2023.
Article published online May 30, 2023.

formed in the pellets plays an important role during melting. Hence, the reaction mechanisms during the melting of H-DRI is important and needs to be studied more thoroughly.

Additionally, this study is based on iron ore pellets that contain 0.1 to 0.2 wt pct vanadium.[12,13] Vanadium slag can constitute a valuable by-product to iron and steel producers, and is therefore interesting to study further. One of the key properties for economically viable vanadium extraction is the concentration of vanadium in the slag. Information on the transfer of vanadium from the H-DRI to the autogenous slag during melting will thus be valuable for the development of a V extraction route from H-DRI slag.

The aim of this study is therefore twofold. First, aiming to increase the understanding of the reaction mechanisms during melting of H-DRI. Secondly, the study aims to increase the understanding of the behavior of V during melting, which will be useful for future studies related to V extraction. With these aims in focus, an experimental study is carried out in which single H-DRI pellets with reduction degrees of 90 and 99 pct heated at 1773 K and 1873 K for different times (60 to 600 seconds), corresponding to different stages of melting. As a starting condition, heat is supplied solely by conduction, which corresponds to a scenario with bad contact to slag and steel. After rapid cooling, the cross sections of the H-DRI pellets are investigated using backscatter electron (BSE) microscopy and electron dispersive spectroscopy (EDS) in a scanning electron microscope (SEM).

II. EXPERIMENTAL

The experiments were carried out in two steps. Industrial iron ore pellets were first reduced in hydrogen and then heated for a range of times to observe the melting progression. The heating of the H-DRI pellets is the focus of this study, hence this setup is described in detail next.

A. *Experimental Setup*

A vertical tube furnace with alumina reaction tube and $MoSi_2$ heating elements was used to heat and melt the samples. Figure 1 is a schematic drawing of the melting furnace. The Ø80 mm reaction tube was connected to a cooling chamber in the upper end, and a cooled cap in the lower end. A steel rod was installed through the top of the cooling chamber. The steel rod was connected to a lifting system to enable the movement of the steel rod up and down inside the furnace. To the lower end of the steel rod, the sample was connected. A thermocouple was inserted through the cap at the lower end of the furnace. The tip of the thermocouple was positioned just below the sample when the sample was in the high temperature zone of the furnace. All connections were gas sealed. The temperature in the high temperature zone was uniform over a length of 5 cm.

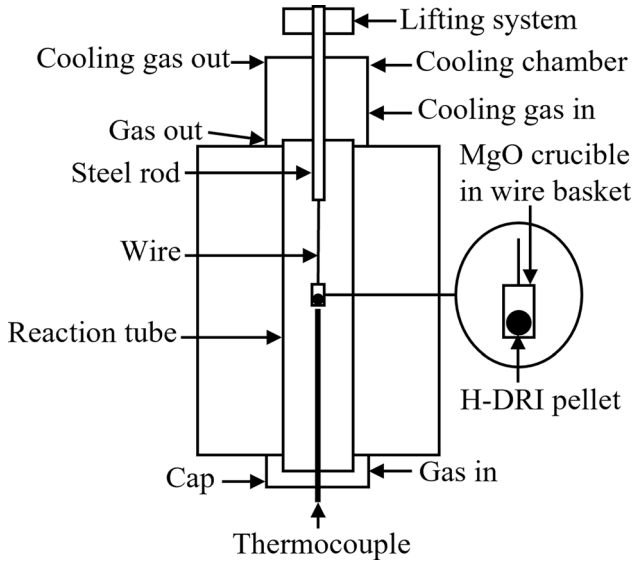

Fig. 1—Schematic drawing of the melting furnace.

B. *Experimental Procedure*

To obtain H-DRI pellets with different reduction degrees, industrial hematite pellets based on apatite iron ore from northern Sweden were reduced at 1173 K by pure hydrogen (2 L min^{-1}) in a sealed vertical tube furnace. The hematite pellets (∅ = 10 to 12.5 mm) contained 67.8 wt pct iron and 3 wt pct non-ferrous oxides.[13] The non-ferrous oxides originate from gangue as well as bentonite and dolomite additions during pelletization. Table I shows the fractions of the major constituents. The reduction degree was calculated by the following equation:

$$\text{Reduction degree(pct)} = \frac{m_1 - m_2}{m_1 - m_{100\,\text{pct}}} \times 100, \quad [1]$$

where m_1 and m_2 are the masses of the pellets before and after reduction, respectively, and $m_{100\ \text{pct}}$ is the mass of the pellet when Fe_2O_3 is reduced to Fe.

After reduction, one pellet was placed in a small MgO crucible. A small basket of Mo wire was used as hanging device for the pellet containing crucible. The masses of the pellet, crucible, and basket were kept constant in all experiments, *viz*. 2, 12, and 0.4 g, to not alter the amount of heat needed for melting the samples. The sample basket was connected to the lower end of the steel rod using 40 cm Mo wire as shown in Figure 1.

The sample was initially positioned in the cooling chamber of the melting furnace. The furnace was closed and ensured gas tight by introducing vacuum. The furnace was then refilled with argon. To ensure that the atmosphere had been sufficiently changed to argon, the furnace was evacuated and refilled with argon gas another two times. After the last refilling, an argon flow of 0.1 L min^{-1} was maintained. The furnace was then heated to a temperature of either 1773 K or 1873 K. When the experimental temperature was reached, the sample was lowered to the high temperature zone where

Table I. Composition of Hematite Pellets in Weight Percent, Showing the Major Constituents

Fe	MgO	Al_2O_3	SiO_2	P_2O_5	CaO	TiO_2	V_2O_3	MnO
67.8	0.65	0.2	0.8	0.06	0.9	0.18	0.2	0.07

Data comes from product catalog.[13]

Table II. Reduction Degrees of H-DRI Along with Experiment Lengths and Temperatures

No.	Reduction (Pct)	Time (s)	Temperature (K)
1	99	60	1873
2	99	90	1873
3	99	120	1873
4	99	240	1873
5	99	600	1873
6	90	60	1773
7	90	120	1773
8*	95	5	1923

*Experiment no. 8 is 3 H-DRI pellets compressed to a cylindrical pellet dropped into liquid iron.

it was kept for a predetermined time, as can be seen in Table II, where the reduction degree of each sample also is stated. The experiment was terminated by lifting the sample rapidly to the cooling chamber, while flushing argon into the cooling chamber to enhance the convection and cooling rate. The flushing was maintained for 30 minutes.

A supplementary experiment was conducted in which a cylindrical pellet of three compressed H-DRI was dropped into a crucible filled with liquid iron, experiment no. 8 in Table II. The liquid iron was held at 1923 K and under argon atmosphere. After 5 seconds, the sample (liquid iron + cylindrical pellet) was cooled in the cooling chamber.

The samples were then prepared for SEM. In addition, one unreduced hematite pellet as well as two un-heated H-DRI pellets of 90 and 99 pct reduction degree were prepared. The microstructures of the samples were examined, and the phase compositions were determined using EDS in at least three different positions in each phase found in the sample. The composition data were used solely for phase characterization, given the limitations of EDS.

III. RESULTS

A. *Phases in Unreduced and Reduced Pellet*

To understand the melting progression of H-DRI, it is essential to know the pellet microstructure before melting. Therefore, to help the discussion, both an unreduced hematite pellet along with two H-DRI pellets of 90 and 99 pct reduction degree were examined prior to heating.

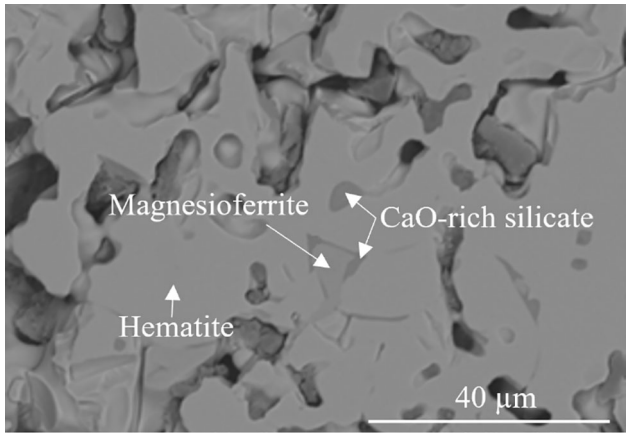

Fig. 2—BSE micrograph of an unreduced iron ore pellet containing hematite, magnesioferrite, and CaO-rich silicates.

The unreduced pellet is found to contain hematite, magnesioferrite, and CaO-rich silicates, as shown in Figure 2. The unreduced pellet also contains apatite, although not shown in Figure 2. In addition to the CaO-rich silicates, the investigated pellets contain a minor amount of other silicates that are not studied here. The phases are identified based on their compositions. They were determined by EDS analysis and are given in Table III. An attempt to use X-ray diffraction (XRD) for phase identification was made, but only hematite was detected due to the small amount of non-ferrous oxides.

The microstructures of the H-DRI pellets prior to heating are shown in Figure 3 (90 pct reduction) and Figure 4(a) (99 pct reduction). Just as the unreduced pellet, these pellets contain apatite and CaO-rich silicates. They also contain wüstite and $CaTiO_3$. Additionally, the 99 pct reduced pellet contains Mg-rich oxides on a 1 μm size. Table IV displays the compositions of the different phases found in the 99 pct reduced pellet. The compositions of the phases found in the 90 pct reduced pellet are similar.

The wüstite phase contains FeO, some MgO and minor amounts of MnO and V_2O_3, given in Table IV. Naturally, the amount of wüstite is much lower in the pellet of 99 pct degree of reduction than in the pellet of 90 pct degree of reduction. This explains why no unreduced wüstite is captured in Figure 4(a).

The Mg-rich oxides on the 1 μm-scale often contain small amounts of other oxides, for example V_2O_3, according to Table IV. They are distributed in clusters as shown in Figure 4(a). Figure 4(b) shows the Mg-rich oxides at a higher magnification.

Table III. Average Compositions of the Phases Present in the Unreduced Hematite Pellet

Phase	MgO, Wt Pct	Al_2O_3, Wt Pct	SiO_2, Wt Pct	P_2O_5, Wt Pct	CaO, Wt Pct	TiO_2, Wt Pct	V_2O_3, Wt Pct	Fe_2O_3, Wt Pct
Magnesioferrite	11 (2)	0 (0)	0 (0)	1 (1)	1 (0)	0 (0)	0 (0)	87 (2)
Hematite	0 (0)	0 (0)	0 (0)	1 (0)	0 (0)	0 (0)	0 (0)	99 (1)
$CaO–SiO_2$	2 (1)	1 (0)	29 (5)	4 (1)	46 (6)	0 (0)	4 (1)	14 (5)
Apatite	0	0	1	39	56	0	0	4

The standard deviations are given in brackets.

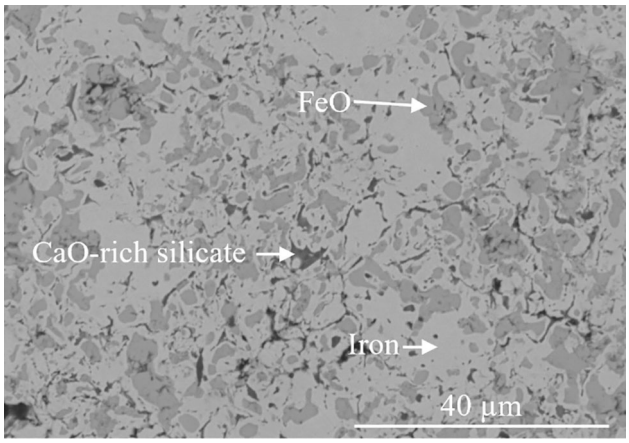

Fig. 3—BSE micrograph of a 90 pct reduced H-DRI pellet containing iron, wüstite, and CaO-rich silicate.

The CaO-rich silicates are found in both Figures 3 and 4. The CaO/SiO_2 mole ratio of the CaO-rich silicates is in the range 0.6 to 2.5, the average being 1.3. Table IV presents the average composition. The CaO-rich silicates also contain small concentrations of other oxides, for example MgO, P_2O_5, and V_2O_3.

The FeO content of the CaO-rich silicates and the Mg-rich oxides varies in a broad range, likely due to interference from the sample background. Note that the oxidation states of iron and vanadium used in Table IV were not determined in this work.

B. *Heating of 90 Pct Reduced Pellet at 1773 K*

Pellets of 90 pct degree of reduction were heated at 1773 K to study the formation of slag. The microstructures after 60 and 120 seconds of heating are shown in Figures 5(a) and (b). Both microstructures are porous. According to Figures 5(a) and (b), the pores constitute a pore network in the pellet. Figure 5(a) shows that the wüstite and the CaO-rich silicates are still separated after 60 s of heating. Figure 5(b) shows that after 120 seconds the wüstite and CaO-rich silicates have reacted and formed a slag. The slag is found in the pore network. The slag consists of two phases, marked as Phase 1 and Phase 2 in Figure 5(b). Phase 1 primarily contains CaO, SiO_2, and FeO, while Phase 2 contains FeO and MgO. The average compositions of these phases according to EDS measurements are shown in Table V.

C. *Melting of 99 Pct Reduced Pellet at 1873 K*

Pellets of 99 pct reduction degree were maintained at 1873 K from 60 to 600 seconds to study the melting process.

Figure 6(a) shows the porous microstructure of the pellet that has been heated for 60 seconds. Iron is not yet molten, while a complex slag phase has formed in the pore network of the pellet. Figure 6(b) shows the phases present in the slag, denoted as Phase 1 to 3. The average compositions of the phases are given in Table V. Based on the phase compositions, it is clear that Phase 1 and Phase 2 in Figure 6(b) are the same as Phase 1 and Phase 2 in Figure 5(b), while Phase 3 contains MgO, V_2O_3, Al_2O_3, and FeO. Furthermore, apatite and $CaTiO_3$ are present, as Figures 6(c) and (d) show.

After 90 seconds, the iron is molten. Slag droplets, up to 1 mm, are present in the liquid metal phase, as shown in Figure 6(e). Additionally, a greater number of smaller slag droplets in the magnitude of 10 μm are found in the liquid metal phase. A slag layer covers the surface of the iron, as shown in Figure 6(e). The same phases as previously described, Phase 1 to 3, are present in the slag layer.

After 120 seconds, the large slag droplets have joined the slag layer forming a bulk slag phase. However, some slag droplets with a maximum size of about 30 μm in diameter are kept in the liquid metal phase, see Figure 6(f).

The oxidic droplets remaining in the iron are after 240 and 600 seconds not larger than 5 μm.

D. *Melting of H-DRI in Liquid Iron*

A cylindrical pellet of three compressed H-DRI pellets was dropped into liquid iron. The compressing of three H-DRI pellets was needed to increase the thermal mass of the H-DRI and allow observations on the melting progression, as one pellet was completely molten after the fastest possible cooling. 5 seconds after the H-DRI is dropped into liquid iron it is not fully melted. Figure 7 shows that at this point, autogenous slag has formed

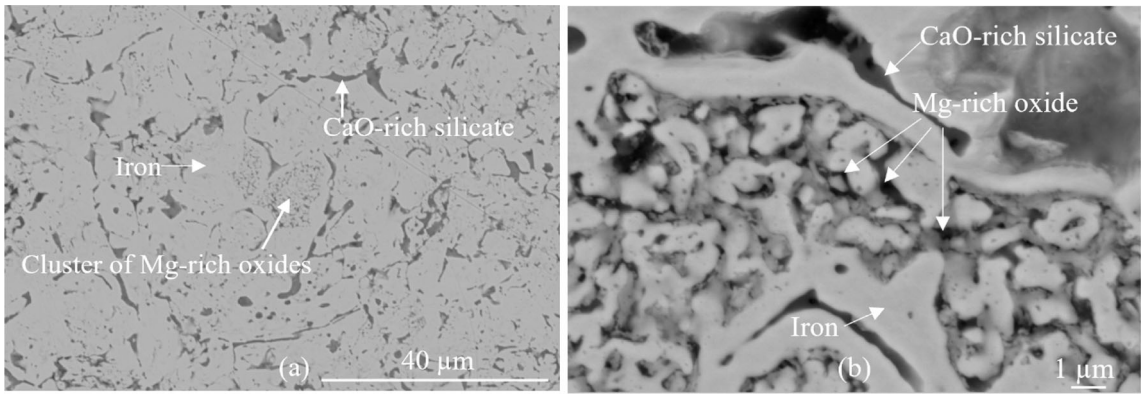

Fig. 4—(*a*) BSE micrograph of a 99 pct reduced H-DRI pellet containing iron, CaO-rich silicate, and clusters of Mg-rich oxides. (*b*) BSE micrograph focusing on the Mg-rich oxides.

Table IV. Average Compositions of the Phases in the 99 pct Reduced Pellet

Phase	MgO, Wt Pct	Al_2O_3, Wt Pct	SiO_2, Wt Pct	P_2O_5, Wt Pct	CaO, Wt Pct	TiO_2, Wt Pct	V_2O_3, Wt Pct	MnO, Wt Pct	FeO, Wt Pct
CaO–SiO_2	2 (1)	1 (1)	21 (9)	1 (1)	26 (15)	0 (0)	1 (1)	1 (0)	48 (25)
Wüstite	9 (5)	0 (0)	0 (0)	0 (0)	0 (0)	0 (0)	1 (1)	3 (3)	87 (8)
Apatite	0 (0)	0 (0)	0 (0)	38 (1)	59 (1)	0 (0)	0 (0)	0 (0)	3 (1)
Mg-rich oxide	16 (10)	4 (5)	0 (0)	0 (0)	0 (0)	2 (3)	2 (1)	1 (1)	76 (7)
$CaTiO_3$	0 (0)	0 (0)	3 (1)	0 (0)	36 (0)	54 (3)	0 (0)	0 (0)	7 (2)

The standard deviations are given in brackets.

throughout the cylindrical pellet. At the interface between the pellet and the liquid iron, droplets of autogenous slag are released.

IV. DISCUSSION

A. *Initial Oxide Phases*

To establish the initial condition, the unreduced sample is studied. The phase compositions acquired by EDS suggest that it contains hematite, magnesioferrite, silicates, and apatite, Table III. Apatite is regarded as a gangue mineral. In the presently studied pellet, the CaO-rich silicates are the most abundant silicates, while other silicates are also present. During pelletization, silicates from gangue or bentonite react with CaO from dolomite, forming the CaO-rich silicates in Figures 3 and 4.[14] The CaO/SiO_2 mole ratio in the CaO-rich silicates varies because of the local CaO/SiO_2 ratio in accordance with Frieland and Erickson.[14] Magnesioferrite forms due to the reaction of MgO in the added dolomite with magnetite during pelletization.[14]

The silicates and the apatite are present in the reduced sample, together with some additional oxide phases, *viz*. FeO, $CaTiO_3$, and Mg-rich oxides. Magnesioferrite and hematite are not present in the reduced samples. The $CaTiO_3$ is identified from the equimolar amounts of CaO and TiO_2, shown in Table IV. This phase originates from the gangue.

As implied by the presence of several oxide phases in the reduced samples, only iron oxide is reduced significantly during reduction. The reduction reaction of a metal oxide Me_xO_y by hydrogen can be written as

$$Me_xO_y + yH_2(g) = xMe + yH_2O(g). \quad [2]$$

If the oxide and its corresponding metal are pure, their activities are 1 and the equilibrium water pressure of the reaction can be calculated using tabulated thermodynamic data.[15] The equilibrium water pressure is high for the reduction of iron oxide compared to the reduction of the other oxides in the sample. It means that for the reduction of the other oxides to proceed, a more efficient removal of water from the reaction site is needed. Dissolution of the metal into iron decreases the activity of the metal, thus allowing a higher water content according to Eq. [2]. On the other hand, the dissolution into iron requires solid state diffusion, which is a very slow process. As a result of the weak kinetic conditions, reduction of the other oxides does not occur. An additional constraint for the reduction of MgO and CaO is the negligible solubility of Mg and Ca in Fe.

The above discussion explains why the silicates, the apatite, and the $CaTiO_3$ are not reduced. It also explains the appearance of the 1 μm Mg-rich oxides inside the iron in Figure 4. The Mg-rich oxides contain MgO, Al_2O_3, V_2O_3, and TiO_2 according to Table IV. These oxides are likely dissolved in the iron oxide lattice. While iron oxide is reduced, these oxides remain oxidic. As

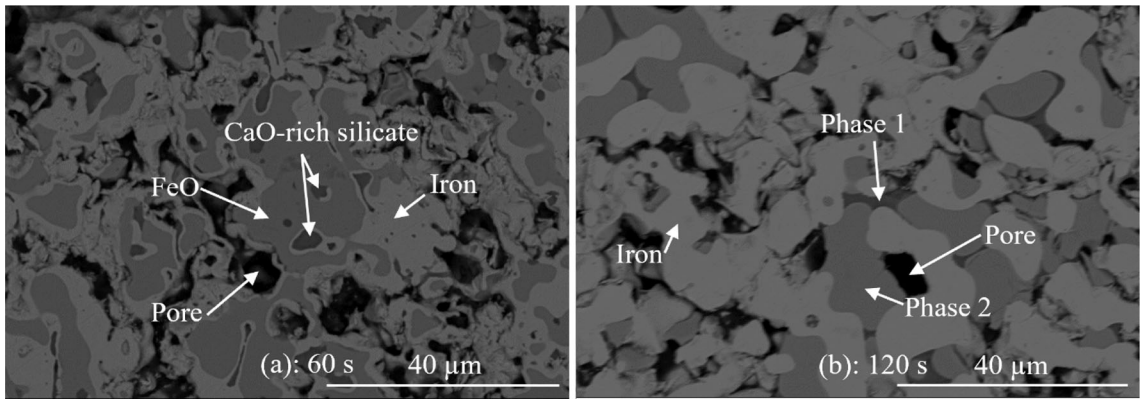

Fig. 5—BSE micrographs of the microstructure of (*a*) a 90 pct reduced pellet after heating for 60 s and (*b*) a 90 pct reduced pellet after heating for 120 s at 1773 K.

they are not reduced, they are found as the Mg-rich oxides after reduction. It is interesting to mention that Kim *et al*. observed similar gangue-related impurities which appear as small oxides in the reduced iron.[16]

B. *Progression of Oxide Phases*

As pellets are heated in the reactor, it is expected that reactions will take place prior to the melting of the metal phase. Therefore, the slag formation in a pellet of 90 pct reduction degree is studied below the melting point of iron.

After 60 seconds of heating, no change is observed in the microstructure as found by comparing Figure 5(a) with Figure 3. The figures also show that FeO initially is in the center of the iron grains, corresponding to not fully reduced iron ore, which is in accordance with Reference 17.

After further heating, a slag forms by the reaction between CaO-rich silicates and FeO, as shown in Figure 5(b). The composition of the two slag phases in Figure 5(b), given in Table V, suggest that they are liquid at 1773 K.[18] It is known that FeO has a melting point below iron, 1650 K compared to 1811 K, while the CaO silicates have melting points above. The CaO silicate with the lowest melting point is $CaO{\cdot}SiO_2$, melting at 1817 K.[19] It is therefore suggested that melting of FeO and subsequent dissolution of CaO-rich silicates is the necessary condition for slag formation in the pellet prior to melting of the metal phase. This is understandable as FeO has high solubility for the CaO-rich silicates.[20] The dissolution of the CaO-rich silicates likely initiates as the FeO flows from the center of the iron grains into the pore network of the pellet, where the slag is found in Figure 5(b). As the amount of FeO is much greater than the total amount of the non-ferrous oxides, it is reasonable to assume that saturation will not be met. In Figure 8, an arrow line in red inserted on a sectioned version of the $CaO–SiO_2–FeO_n$ phase diagram denotes how the liquidus temperature changes when FeO dissolves CaO-rich silicates with a CaO/SiO_2 mole ratio of 1.3, which is the average of the CaO-rich silicates (Table IV). It is seen that 10 wt pct FeO is enough to fully dissolve such CaO-rich silicate at 1673 K. Given the earlier observation that the same type of industrial pellets generates an autogenous slag containing 73 wt pct FeO when the reduction degree is 91 pct,[9] it is reasonable to expect complete dissolution of the CaO-rich silicates in FeO in the present study. This explains how the slag can be formed before iron melts. Furthermore, the amount of iron oxide decreases as the degree of reduction increases. Thus, the 99 pct reduced pellet is studied, which according to mass balance calculations contains only 10 pct of the amount of FeO in the 90 pct reduced pellet. The autogenous slag of 99 pct reduced pellets was found to contain 22 wt pct FeO experimentally.[9] Even though the amount of iron oxide is very low, the 99 pct reduced pellet also shows the formation of slag prior to the melting of iron, as seen in Figure 6(a). The investigated samples can be treated as boundary conditions since the industrial reduction shaft most likely will aim on a reduction degree between 90 and 99 pct.

The Mg-rich oxides that were found before melting in the 99 pct reduced sample disappear when the slag is formed, indicating that they have dissolved into the slag.

As the metal phase melts, the slag coalesces and forms droplets as in Figure 6(e) to minimize the interfacial energy. Both the apatite and $CaTiO_3$ that are present until iron melts according to Figures 6(c) through (d) dissolve in the slag. Huss *et al*. studied the dissolution of apatite in a separate work and explained that the melting of iron increases the mobility of the slag so that a sufficient amount of slag can dissolve the apatite.[11] The same theory can likely be applied on the dissolution of $CaTiO_3$.

The largest slag droplets flow to the surface of the liquid metal forming the initial slag layer as shown in Figure 6(e). As the buoyancy force of a larger droplet is greater than for a small droplet, the sizes of the slag droplets decrease with prolonged heating, Figure 6(f). As flotation continues, almost all slag joins the top slag.

In an industrial process, the pellets will most likely be continuously fed to the reactor. The pellets can then end up in different positions in the furnace. If the pellets float on top of a highly viscous slag, the heat transfer to the pellets will be poor, while if they sink through the slag and meet the liquid steel, the heat transfer will be fast. This study has been focusing on H-DRI melting

Table V. Average Compositions of the Slag Phases in the Heated H-DRI of 90 and 99 Pct Reduction Degree

Reduction Degree, pct	Slag Phase	MgO, Wt Pct	Al_2O_3, Wt Pct	SiO_2, Wt Pct	P_2O_5, Wt Pct	CaO, Wt Pct	TiO_2, Wt Pct	V_2O_3, Wt Pct	MnO, Wt Pct	FeO, Wt Pct
90	1	3	5	33	1	33	1	0	0	24
90	2	3	0	0	0	0	1	1	0	95
99	1	9	5	32	1	34	2	0	1	15
99	2	19	1	0	0	0	1	5	1	73
99	3	14	12	1	0	1	13	28	3	29

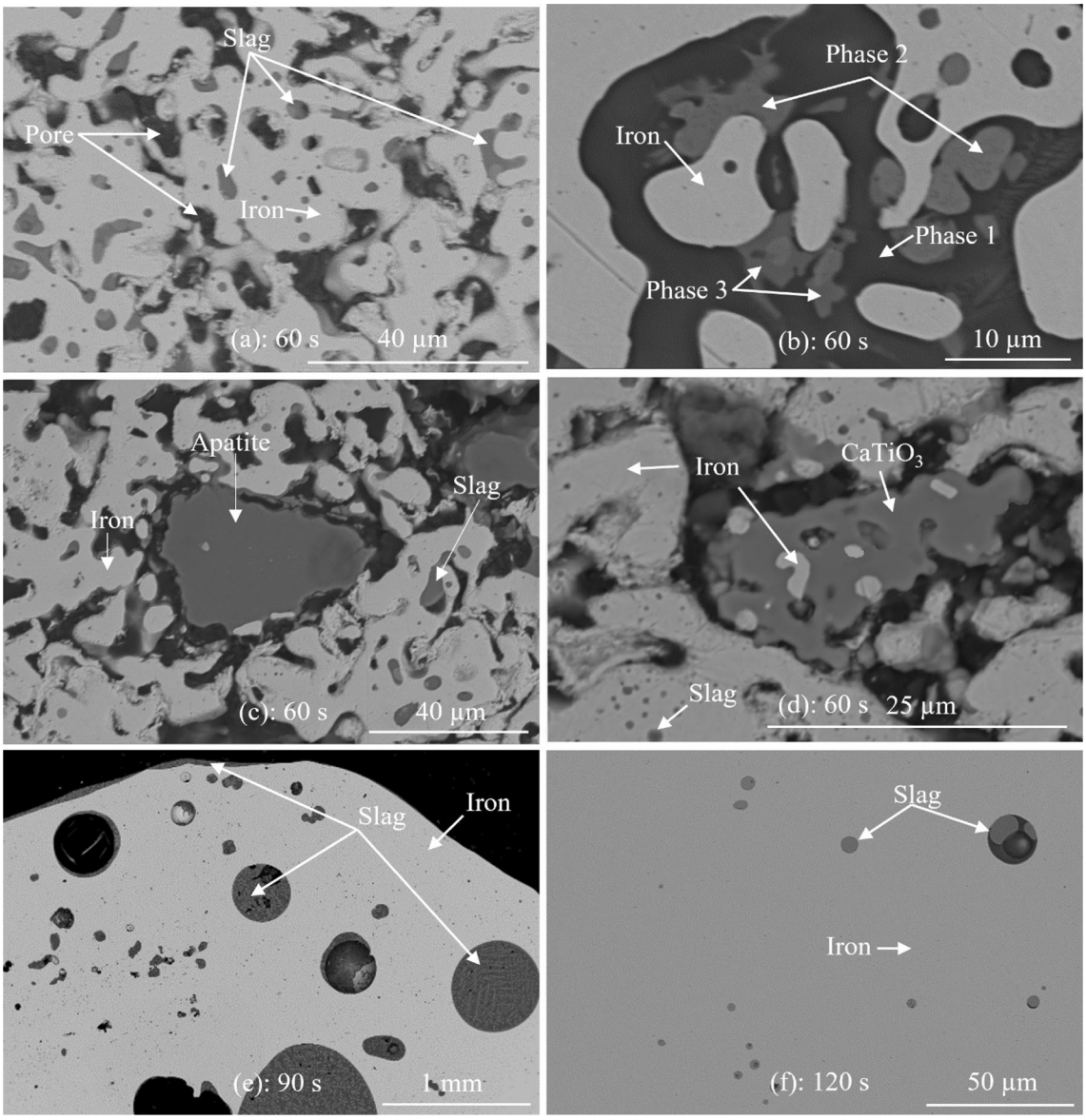

Fig. 6—BSE micrographs of the microstructures at different stages of melting of pellets of 99 pct reduction degree. (*a*), (*b*): autogenous slag in the pore network after heating for 60 s, (*c*), (*d*): apatite and $CaTiO_3$ present after 60 s, (*e*): melting of iron and floating up of coalesced slag after 90 s, (*f*): slag droplets in the liquid iron after 120 s.

with poor contact to slag or steel. To extend the present observations on the progression of melting of H-DRI, three H-DRI pellets were compressed to a cylindrical pellet and dropped into a bath of liquid iron. The result is shown in Figure 7 and confirms the formation of autogenous slag prior to the melting of iron inside the

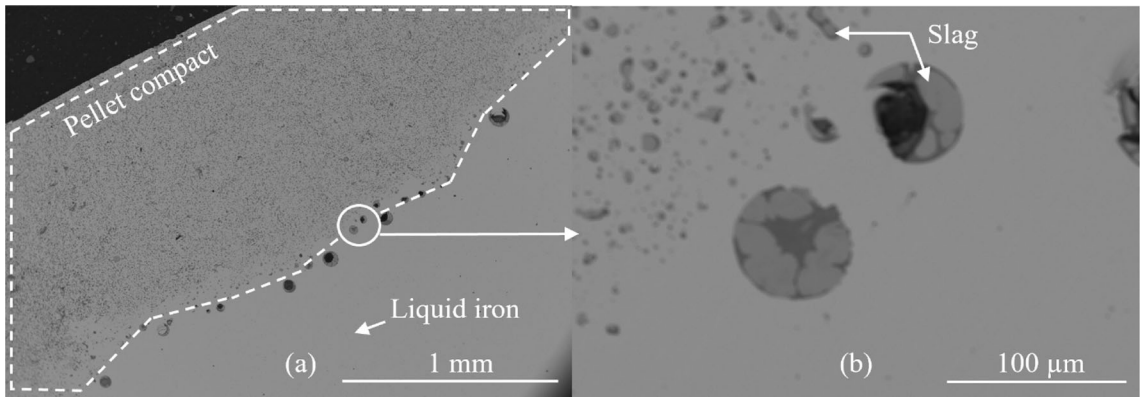

Fig. 7—BSE micrographs showing (*a*) the formation of autogenous slag in the not fully melted H-DRI and (*b*) the release of autogenous slag into the liquid iron.

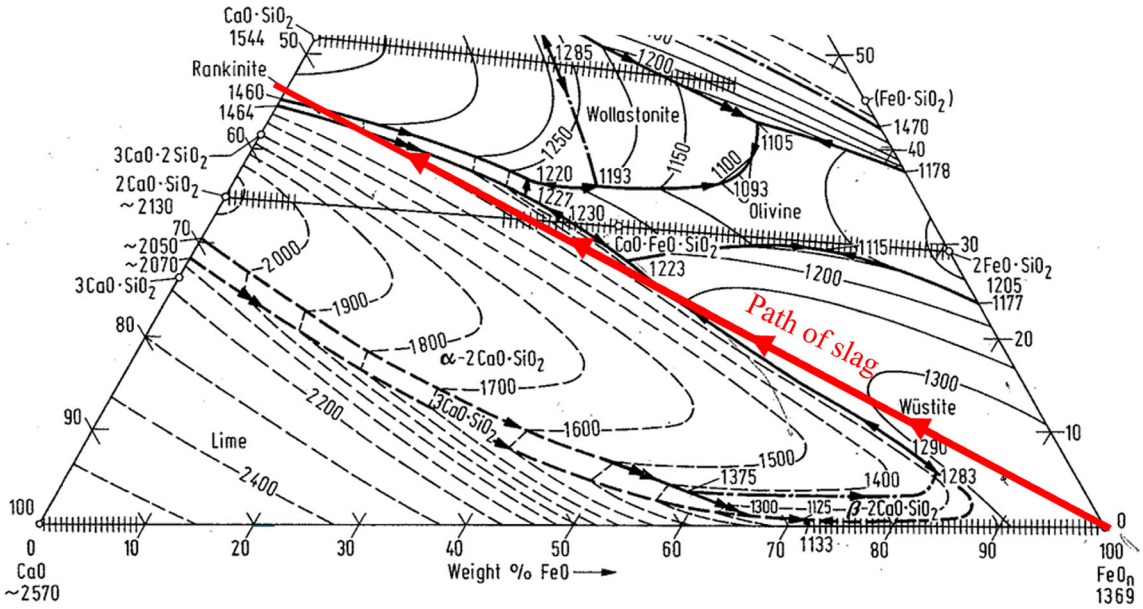

Fig. 8—The liquidus temperature change when FeO dissolves a CaO-rich silicate with average molar CaO/SiO_2 = 1.3 follows the arrow line that has been inserted on the sectioned $CaO–SiO_2–FeO_n$ phase diagram, originally from Slag Atlas.[19] The temperature is given in °C.

H-DRI. This demonstrates that the suggested melting progression of H-DRI is relevant to several scenarios that can occur in the industrial process.

C. *Vanadium*

A particular interest is taken in the progression of vanadium-containing phases. It will therefore be discussed in detail. Vanadium is present in the magnetite phase lattice in the ore.[12] During the pelletization process, magnetite is oxidized to hematite at 1523 K to 1623 K.[21,22] To the knowledge of the present authors, no description of what happens to vanadium during oxidation of the ore exists in the literature. It is possible that some of the vanadium remain in the hematite lattice after the pelletization process, since the phase diagram between V_2O_5 and Fe_2O_3 shows solubility of 6 mol pct V_2O_5 in Fe_2O_3 in air atmosphere at 1573 K.[23] This cannot be reliably confirmed with EDS due to the low content of vanadium in the magnetite raw material (0.1 to 0.2 wt pct)[12] and the limitations of EDS analysis.

Table III shows that V is present in the CaO-rich silicates before reduction. It implies that it is possible for V to diffuse to the CaO-rich silicates from the magnetite lattice under the pelletization conditions, since the dolomite and bentonite added during pelletization contains little V. After reduction, vanadium is present in the Mg-rich oxides, in the CaO-rich silicates and in FeO, according to Table IV. The formation of the Mg-rich oxides was discussed earlier. The presence of V in the Mg-rich oxides and in FeO indicates that while some V diffuses to the CaO-rich silicates during

pelletization, some V remains in the hematite lattice. Hence, the V contained in the hematite lattice will stay in the remaining oxidic phases that precipitate during reduction, as seen by Kim *et al*.[10]

The progression of vanadium during melting is studied using a sample of 99 pct reduction since the lower FeO content gives a higher concentration of V in the slag.[9] Already after short time of heating (60 seconds), vanadium is found in the magnesiowüstite and the Al_2O_3–FeO–MgO–TiO_2–V_2O_3-containing spinel, shown in Figure 6(b) and Table V, which is in accordance with the previous work.[9] These precipitated phases all origin from the FeO, CaO-rich silicates, and Mg-rich oxides that are present after reduction. Hence, under the current oxygen potential, V is more likely to go into these oxidic forms rather than be reduced and dissolved to the iron.[9] Lack of thermodynamic data makes it difficult to predict which V-containing phases are present at different oxygen potentials, more studies are needed in this area. Also, for future V extraction studies, it would be interesting to study which of these phases are more favorable to facilitate the extraction.

V. SUMMARY

The melting progression of hydrogen reduced iron ore pellets was investigated, focusing on the formation of the autogenous slag and how vanadium is transferred from the reduced pellet to the slag. The investigation was carried out by heating, melting, and freezing of hydrogen reduced industrial hematite pellets (H-DRI).

Before melting, the H-DRI was found to contain several oxide phases, namely FeO, CaO-rich silicates, apatite, $CaTiO_3$, and Mg-rich oxides. It was found that the Mg-rich oxides form during reduction and that they appear at high reduction degree (99 pct). Vanadium was detected in the CaO-rich silicates, in the Mg-rich oxides and in FeO.

Melting was found to involve two steps: (1) slag formation and (2) melting of iron.

(1) Before iron melted, all slag movement was restricted to the pore network of the pellet. The slag formation was found to start with FeO melting and flowing out of the iron grains, reacting with the CaO-rich silicates. As the Mg-rich oxides disappeared, it was assumed that they dissolved in the slag.
(2) The melting of iron enabled bulk movement of the slag. The slag coalesced into larger slag droplets to reduce the metal/slag interface. The buoyancy force, and hence the flotation speed, of larger slag droplets was higher. The floatation of slag created a slag layer on top of the molten iron. Small slag droplets, <5 μm, remained in iron after 600 seconds.

V was transferred from the CaO-rich silicates, Mg-rich oxides, and FeO to the slag in step (1).

CONFLICT OF INTEREST

No potential conflict of interest was reported by the authors.

FUNDING

Open access funding provided by Royal Institute of Technology.

REFERENCES

1. P. Wang, M. Ryberg, Y. Yang, K. Feng, S. Kara, M. Hauschild, and W.-Q. Chen: *Nat. Commun.*, 2021, https://doi.org/10.1038/s41467-021-22245-6.
2. S. Zhang, B. Yi, F. Guo, and P. Zhu: *J. Clean. Prod.*, 2022, vol. 340, p. 130813. https://doi.org/10.1016/j.jclepro.2022.130813.
3. J. Tang, M. Chu, F. Li, C. Feng, Z. Liu, and Y. Zhou: *Int. J. Miner. Metall. Mater.*, 2020, vol. 27, pp. 713–23. https://doi.org/10.1007/s12613-020-2021-4.
4. W. Liu, H. Zuo, J. Wang, Q. Xue, B. Ren, and F. Yang: *Int. J. Hydrogen Energy*, 2021, vol. 46(17), pp. 10548–69. https://doi.org/10.1016/j.ijhydene.2020.12.123.
5. W. Kim and I. Sohn: *Joule*, 2022, vol. 6(10), pp. 2228–32. https://doi.org/10.1016/j.joule.2022.08.010.
6. V. Vogl, M. Åhman, and L.J. Nilsson: *J. Clean. Prod.*, 2018, vol. 203, pp. 736–45. https://doi.org/10.1016/j.jclepro.2018.08.279.
7. Y. Yang, K. Raipala, and L. Holappa: *Treatise on Process Metallurgy*, Elsevier, Oxford, 2014, p. 50.
8. R. Selin: *The Role of Phosphorus, Vanadium and Slag Forming Oxides in Direct Reduction Based Steelmaking*, The Royal Institute of Technology, Stockholm, 1987, pp. II:5–33. ISSN 0284-3013.
9. A. Vickerfält, J. Martinsson, and D. Sichen: *Steel Res. Int.*, 2021, vol. 92, p. 2000432. https://doi.org/10.1002/srin.202000432.
10. O. Hessling, M. Tottie, A. Vickerfält, J. Martinsson, N. Kojola, D. Sichen: *Proc. Int. Conf. Molten Slags, Fluxes Salts* 21, 11th, 2021.
11. J. Huss: Swerim AB, Stockholm, unpublished research, 2023.
12. S. Landergren: *On the geochemistry of Swedish iron ores and associated rocks*, AB Kartografiska institutet. Esselte AB, Stockholm, 1948, p. 80.
13. *2021 products*, LKAB, 2021, p. 23.
14. J.J. Frieland and E.S. Erickson Jr.: *Metall. Trans. B*, 1980, vol. 11B, pp. 233–43.
15. E.T. Turkdogan: *Physical Chemistry of High Temperature Technology*, Academic Press, New York, 1980.

16. S.H. Kim, X. Zhang, Y. Ma, I.R.S. Filho, K. Schweinar, K. Angenendt, D. Vogel, L.T. Stephenson, A.A. El-Zoka, J.R. Mianroodi, M. Rohwerder, B. Gault, and D. Raabe: *Acta Mater.*, 2021, vol. 212, p. 116933. https://doi.org/10.1016/j.actamat.2021.116933.
17. O. Hessling, J. Brännberg Fogelström, N. Kojola, Du Sichen: *Metall. Mater. Trans. B*, 2022, pp: 1–11.
18. ThermoCalc Software 2021a.
19. *Slag atlas*, Verein Deutscher Eisenhüttenleute, Düsseldorf, 1981.
20. T. Hidayat, D. Shishin, S.A. Decterov, and E. Jak: *Calphad*, 2017, vol. 56, pp. 58–71.
21. S. Lúcia de Moraes, J.R. Baptista de Lima, T. Ramos Ribeiro: *Iron Ores and Iron Oxide Materials*, IntechOpen, 2018, Ch. 3. https://doi.org/10.5772/intechopen.73164.
22. Y. Yang, K. Raipala, and L. Holappa: *Treatise on Process Metallurgy*, Elsevier, Oxford, 2014, p. 21.
23. W. Dutoit Malan, G. Akdogan, P. Taskinen, J. Hamuyuni, and J. Zietsman: *Calphad*, 2018, vol. 63, pp. 12–23. https://doi.org/10.1016/j.calphad.2018.08.003.